Accepted Manuscript

Alkali activated composites – An innovative concept using iron and steel slag as both precursor and aggregate

Nuno Cristelo, João Coelho, Tiago Miranda, Ángel Palomo, Ana Fernández-Jiménez

PII: S0958-9465(19)30182-9

DOI: https://doi.org/10.1016/j.cemconcomp.2019.04.024

Reference: CECO 3308

To appear in: *Cement and Concrete Composites*

Received Date: 13 February 2019

Revised Date: 18 April 2019

Accepted Date: 23 April 2019

Please cite this article as: N. Cristelo, Joã. Coelho, T. Miranda, Á. Palomo, A. Fernández-Jiménez, Alkali activated composites – An innovative concept using iron and steel slag as both precursor and aggregate, *Cement and Concrete Composites* (2019), doi: https://doi.org/10.1016/j.cemconcomp.2019.04.024.

April 2019 R1

Alkali activated composites – an innovative concept using iron and steel slag as both precursor and aggregate

[a,*] Nuno Cristelo; [b] João Coelho; [c] Tiago Miranda; [d] Ángel Palomo; [e] Ana Fernández-Jiménez

[a] CQ-VR, Department of Engineering, University of Trás-os-Montes e Alto Douro, 5001-801 Vila Real, Portugal
E-mail address: ncristel@utad.pt
Telephone: + 351 259 350 383
[*] Corresponding author

[b] Department of Civil Engineering, University of Minho, 4800-058 Guimarães, Portugal
E-mail address: id7225@uminho.com

[c] ISISE, Institute of Science and Innovation for Bio-Sustainability (IB-S), Department of Civil Engineering, University of Minho, 4800-058 Guimarães, Portugal
E-mail address: tmiranda@civil.uminho.com

[d] Instituto Eduardo Torroja (IETcc), CSIC, C/Serrano Galvache 4, 28033 Madrid, Spain
E-mail address: palomo@ietcc.es

[e] Instituto Eduardo Torroja (IETcc), CSIC, C/Serrano Galvache 4, 28033 Madrid, Spain
E-mail address: anafj@ietcc.es

ABSTRACT

The present paper addresses the feasibility of using an iron and steel slag aggregate (ISS), resulting from electric arc furnace, as a recycled raw material in the production of a new concept of mortar composite, based on alkaline activation, designated as 'alkali activated composite' (AACO). The original ISS aggregate was used both as a precursor and an aggregate, either as received (aggregate fraction) or after mechanical activation (precursor fraction). In the first stage, to determine its potential as a precursor, it was mixed with fly ash (FA), using weight ratios of 100/00, 75/25, 50/50, 25/75 and 00/100. The most effective results were obtained with the blend 50/50, which was subsequently used to study the performance of the aggregate fraction. The second stage was comprised of tests on the mortar composites, combining some of the previously tested pastes with the ISS or with a normalised sand (for reference). A 8M sodium hydroxide solution was used as the activator for all pastes and mortars tested. The curing developed throughout 2 or 28 days, at 22ºC, after an initial 20h period at 85ºC. The reaction products were characterised using X-Ray Diffraction and microscopy (scanning electron microscopy, for the pastes, and back-scattering electron microscopy, for the mortars). Results show that, indeed, the ISS can be applied as a precursor and/or as an aggregate in the production of alkaline composites.

Key words: Alkali activated composites, iron and steel slag; waste recycling; sustainability

1. Introduction

The iron and steel making sector is strongly characterised by the fact that it recycles all the available steel, being regarded as an excellent example of circular economy, maintaining, and even increasing, the value of its products. Moreover, steel is capable of adapting to the necessities of modern products, since it can be endlessly recycled without losing any of its properties. However, during the fabrication process, a significant volume of slag is generated, with a significant percentage being landfilled. It is estimated that 400 kg of slag are accumulated per ton of steel manufactured [1].

Slag is essentially the sum of the impurity content in the raw material, after the extraction of the ore, and the previously added materials (e.g. lime to produce a more fluid slag); or in the molten pig iron, during the steel refining process. The production of iron and steel slag can thus be divided in two main phases, i.e. blast furnace slag and steel-making slag. The first results from the smelting of iron ore in a blast furnace (BF), from which the pig iron (also known as crude iron) is generated. That slag can be air-cooled (resulting in a rock-like material) or water-cooled (resulting in a fine particle or granulated material). The second type of slag results from basic oxygen furnaces (BOF) and electric arc furnaces (EAF), and the EAF slag can be further divided in the oxygen converter process slag and deoxidation process slag [2]. A third type of slag is usually generated when additional impurities are removed from the molten steel, during transportation in a ladle (usually if slag pits, for cooling, are not available near the EAF). The slag produced at this stage is called ‘ladle slag’ and must be kept separated from the EAF slag, due to significant differences in composition promoted by the several additives applied.

In 2016, over 1 600 million tons of crude steel were produced worldwide, with 25% (over 415 million tons) obtained through EAF [3]. Therefore, it is not surprising that over 400 million tons of different types of iron and steel slag are produced, worldwide, per year, and to produce 1 tonne of EAF crude steel, approximately 200 kg of by-products are generated, of which 90% are EAF slag [4], the type used in the present study. These significant values form a sufficiently solid reason to study, in depth, alternative destinations and technologies that can enable the reuse of this industrial by-product.

The increase in the exploitation of natural resources and of the CO_2eq emissions that are attributed to the construction industry are two factors that keep pushing the boundaries of R&D investment regarding alternative, more sustainable materials. Several examples of this increasing interest can be found in the literature, especially regarding the application of ladle furnace slag (LFS) as a precursor, in the fabrication of alkali activated cements (AAC), and EAF slag as an aggregate, in the fabrication of concrete and mortars.

Wang *et al.* [5] activated LFS with a 10 M NaOH solution, and concluded that the workability and compressive strength increase with the alkali agent content, while the shrinkage also increases. Bignozzi *et al.* [6] studied the fabrication of AAC with the partial substitution of the metakaolin (precursor) by ladle furnace slag (LFS), using only particles above 0.1 mm. The activating solution was a 1:1 weight combination of sodium silicate and sodium hydroxide (8 M). It was discovered that the LFS, although mainly crystalline, still possess some amorphous content, partially contributing to the formation of the C-(N)-A-S-H binding gel. Additionally, the increasing addition of LFS was responsible for a decrease in the total open porosity, which favoured mechanical strength. Recently, Nguyen *et al.* [7] studied the inclusion of polypropylene fibres in alkali-activated LFS pastes to

improve its brittle behaviour. The LFS was previously milled (up to a d_{50} of less than 10 μm), and was activated with a combination of Na_2SiO_3 and KOH, in solution form. The flexural and compressive strength of both unreinforced and fibre reinforced pastes clearly showed the reactivity and capacity of the LFS to act as a precursor in alkaline cements (e.g. compressive strength values between 70 and 80 MPa were achieved, always under room-temperature curing).

The application of EAF slag in concrete, as an aggregate, was tested by several authors who, in general, compared the mechanical, rheological and durability performance of concrete fabricated with natural aggregates and steel slag aggregates. Biskri *et al*. [8] studied the influence of such recycled aggregates on High Performance Concrete, and concluded that the superior mechanical behaviour attained with EAF slag, compared with limestone coarse aggregates, was due to its higher cement-aggregate adhesion. Coppola *et al*. [9] partially replaced different types of natural aggregate (fine sand, fine gravel and coarse gravel) with increasing percentages of EAF slag aggregates (with particle sizes similar to those of the natural aggregate) and concluded that the higher the content of recycled slag the higher the density, Young's Modulus and compressive strength of the concrete. However, in this case, the dry shrinkage of the concrete also increased. A similar conclusion was obtained by Khan *et al*. [10], who discovered that the substitution of traditional coarse aggregate (basalt) by EAF slag, in concrete mixtures using fly ash (90%) and ground granulated blast furnace slag (10%) as precursors, produced higher compressive strength. Lee *et al*. [11] studied the structural response of reinforced concrete columns fabricated with varying contents of EAF slag aggregate. The results showed that the ductility of these columns, after reaching their ultimate strength, was superior to that of

the columns fabricated with natural aggregates, while also showing less crushing at the ends and delayed plastic hinge formation.

However, although there are many studies focusing on potential applications of EAF slag in the construction industry, it is noteworthy that most of these studies concern its use as a natural aggregate substitute. This is mostly because EAF slag is generally assumed to be inert and crystalline, and thus is not effective as a supplementary cementitious material in traditional Portland cement or other cement blends. Only a few exceptions can be found in the literature. A recent study, conducted by Ozturk *et al.* [12], focused on the effects of the silicate modulus, sodium concentration, curing conditions and curing time on strength and microstructure of EAF slag (with a very similar chemical composition to the material used in the present study), activated with sodium hydroxide and sodium silicate solutions. The main conclusion was that the EAF slag can be effectively activated, supported on compressive strength values up to 22 MPa, after 12h at 80ºC. Another example of the success of EAF slag as a precursor was attained by Nikolic *et al.* [13], who studied the kinetics of dissolution of EAF slag in NaOH and KOH solutions, with a special emphasis on the dissolved Al and Si contents considering the alkaline ion type (NaOH and KOH), the alkali concentration and the temperature during dissolution. Results showed that both Al and Si were dissolved more effectively with an increase in alkali concentration and temperature, and a decrease in the solid/liquid ratio. The NaOH was able to dissolve more Si than the KOH, while the KOH dissolved more Al.

Despite these examples already pointing towards an effective performance of iron and steel slags (ISS) in a precursor role, its application is still far from being clarified or totally understood, justifying the definition of a more objective framework, addressing the

conditions in which the ISS can, and should, be applied as a Portland cement substitute. Furthermore, its simultaneous application as a precursor and an aggregate hasn't, to the best of our knowledge, been proposed. Therefore, the aim of the present paper is to study the feasibility of using a common ISS as the main source of (recycled) raw material for the production of a new concept of mortar, which, since it can be considered an evolution from the alkali activated cements (AAC), was designated by 'alkali activated composite' (AACO). The ISS was either used as received (precursor role) or was mechanically activated (by milling). The first stage focused on the performance of ISS and FA blend pastes, using compressive strength tests, Scanning Electron Microscopy (SEM) and X-ray Diffraction (XRD). In the second stage, coarse ISS or normalised silica sand were added to the previous pastes, and the resulting materials were submitted to compressive strength tests and Back-scattered Electron Microscopy (BSEM).

2. Materials and methods

2.1. Materials

The slag studied in the present paper (Figure 1) is known, in Portugal, as "Inert Steelwork Aggregate for Construction". It is produced by the Portuguese national ironworks, located in Maia, as a result of scrap melting in an electric arc furnace. The fly ash (FA), also used in this study, was provided by the company PEGOP, responsible for the Portuguese thermo-electric power plant located in the village of *Pego*.

Figure 1: (a) Original slag (ISS, as received in the laboratory, and used as an aggregated) and (b) milled slag (ISS-M, used as a precursor)

The chemical composition of the two materials, obtained by X-ray fluorescence (XRF), on a PHILIPS PW-1004 X-ray spectrometer, is shown in Table 1, together with the mass loss on ignition (L.O.I.), between 100 and 1000ºC, for 1 h, using a platinum crucible. The main elements of the ISS are iron oxide (32%), calcium oxide (27%), and silica (20%). The FA presented mostly silica (60%) and alumina (21%) and, based on its chemical composition and the criteria specified in ASTM C618 [14], it was classified as a Class F.

Table 1: Chemical composition of the ISS and FA

Element	ISS (wt%)	FA (wt%)
Al_2O_3	8.91	20.82
CaO	26.73	1.84
Cr_2O_3	1.70	0.02
Fe_2O_3	32.33	8.62
K_2O	0.23	2.75
MgO	4.27	1.94
MnO	3.25	0.06
Na_2O	0.30	1.08
SiO_2	20.29	60.00
SO_3	0.29	0.88
Outros	1.64	1.64
L.O.I.	0.07	0.34

The particle size distribution (PSD) of the original ISS (as received in the laboratory) was obtained by sieving [15] and is presented in Figure 2. In its original state (i.e. as received in the laboratory), this material was used as an aggregate. The PSD of the normalised silica

sand (NSS), used here as a reference aggregate, is shown in the same figure. A density of 3.54 g/cm^3 and a water absorption of 1.68% were attained for the ISS, (EN 1097-6), while the NSS presented a density of 2.64 g/cm^3 and a water absorption of 0.02 %.

The ISS was also milled in the laboratory (ISS-M), until a total of 80% of the particles were lower than 80 microns and 62% lower than 45 microns. The milling was obtained using a purposely designed ball mill, with an increased capacity of 5 kg. The fly ash that was used as a reference precursor (FA-M) was previously milled in a RETSCH RS200, for 3 minutes, at 1200 rpm. The PSD of both precursors (also included in Figure 2) were determined by laser granulometry, on a Sympatec Helos BF analyser, able to measure particles from 0.9 to 175 μm, and using Fraunhofer diffraction theory. The analyses were conducted after a 5-minute ultra-sonic bath, on a water-ethanol solution, for increased particle dispersion.

Figure 2: Particle size distribution of the precursor (FA-M, ISS-M) and aggregate (NSS, ISS) materials

With respect to the mineralogical composition, the X-Ray diffractogram of the ISS-M detected the presence of melilite, magnetite and wustite, while the FA-M presented quartz and mullite as the most important crystalline phases. The diffractogram of the FA-M showed the presence of a halo between angles 17 and 33 (º2θ), revealing the presence of an important vitreous phase in these materials. A similar indication of the presence of material

with a significant amorphisation level was also obtained for the ISS-M, with a halo approximately between 28 and 38 (º2θ), although less pronounced than the one registered for the FA-M (see Figure 4).

A sodium hydroxide solution, with a concentration of 8 M, was used as activator. It was prepared 4 to 6 h before the fabrication of the specimens. Deionised water was used throughout the entire experimental work.

2.2. *Preparation and mechanical testing*

Two different types of mixture were tested: paste and mortar (Table 2). The study of the pastes (i.e. with and without fly ash) allowed the comparative study of the reactivity of the ISS-M as a precursor, and to choose the most interesting binder, in terms of mechanical behaviour. Preparation of the pastes started with the dry mixing of the solid precursors (ISS-M and FA-M), for 5 min, in a Hobart counter mixer. The activator was then slowly added, and an additional mixing period of 3 min followed, to guarantee adequate homogenisation. The activator temperature at the time of the mixing was 20ºC ± 1ºC. The resulting paste was poured inside stainless-steel moulds, with nominal dimensions of 10x10x60 mm.

An activator / precursor ratio of 0.28 was used with the 100S, 75S25F and 50S50F pastes. This value increased to 0.35 for the pastes 25S75F and 100F, to obtain a similar workability, since the initial tests showed that a 0.28 ratio resulted in excessively dry pastes, which were impossible to homogenise properly. This significant rheological

247 difference was due to the differences in the PSD of the ISS-M and FA-M precursors, i.e. as
248 the finer FA-M content increased, so did the liquid phase requirements.
249
250 Table 2: Identification and composition of the pastes and mortars (Ac: activator)

Type	Mixture ID	Binder			ISS / Binder (wt.)	NSS / Binder (wt.)
		Precursor (Pr)		Ac / Pr (wt.)		
		ISS-M (wt%)	FA-M (wt%)			
Paste	100S	100	-	0.28	-	-
	75S25F	75	25	0.28	-	-
	50S50F	50	50	0.28	-	-
	25S75F	25	75	0.35	-	-
	100F	-	100	0.35	-	-
Mortar	100F(ISS)	-	100	0.55	-	3
	50S50F(ISS)	50	50	0.55	-	3
	100F(NSS)	-	100	0.55	3	-
	50S50F(NSS)	50	50	0.55	3	-

251
252 The effect of the ISS as an aggregate was determined by testing 40x40x160 mm mortar
253 specimens [16], with an aggregate / binder ratio of 3/1. Similar mixtures were tested using
254 NSS as an aggregate, for comparison purposes (Table 2). The liquid / solid ratio (i.e.
255 activator / precursor ratio) used to fabricate the composite mortars was 0.55, to guarantee
256 the exact same conditions. This value was established using slump tests [17] on the mortar
257 with the highest water adsorption, i.e. 100F(ISS), to determine the minimum water content
258 required to achieve an adequate workability. Therefore, this particular mortar was prepared
259 with the optimum activator / precursor ratio, but the remaining mortars were prepared with
260 a water content slightly higher than required, which probably influenced its mechanical
261 behaviour, as discussed further ahead. It should also be noted that the water absorption of
262 the original ISS (1.68%) was higher than that of the NSS (0.02%).
263
264 Both pastes and mortars were cured, for the first 20h, inside the moulds, at 85ºC and 99%
265 RH. After that, every specimen was removed from the respective mould and stored, inside
266 the humidity chamber, for the remainder of the curing period – 2 and 28 days (pastes) and

3 and 28 days (mortars). After curing, their compressive strength was determined in an IBERTEST AutoTest-200/10. Each specimen was weighted and measured shortly before being tested. Results showed in this paper represent the average of six tested specimens.

Some pastes were selected for further microstructural characterization, using SEM and XRD, while the mortars were studied using BSEM. The SEM and BSEM analyses were performed on a Hitachi S-4800 scanning electron microscope (20 kV), in low vacuum mode (1.3 mbar), avoiding the deposition of a conductive layer. The device was fitted with a solid-state BSE detector and a X-ray energy dispersive analyser (EDX) – Oxford LINK-ISIS – using a ZAF correction model for quantitative chemical analysis. The XRD used was a BRUKER D8 Advance diffractometer, with CuKα radiation and using 40kV, fitted with an X'Celerator detector and secondary monochromator. The scans covered a 2θ range of 5 to 60º, with a nominal step size of 0.017º and 100 s/step.

3. Results and discussion

3.1. Mechanical behaviour

The uniaxial compressive strength (UCS) of the pastes and mortars, after 2 and 28 days curing, is presented in Figure 3. Regarding the pastes, the 2 and 28-day curing values showed a similar pattern, i.e. the combination of FA-M and ISS-M was more effective than either of these two components alone. The most performing paste was a mixture of 50% FA-M and 50% ISS-M (50S50F). This shows that the milled ISS is, indeed, reactive, and thus can be activated. The fact that the best paste is a combination of both precursors

suggests some level of synergy between them, which is confirmed in Section 3.2, when analysing the element composition of the paste/aggregate interfaces.

Figure 3: Uniaxial compressive strength of the pastes (a) and mortars (b)

The 50S50F and 100F pastes were then chosen to study the behaviour of the ISS as an aggregate. Additionally, reference mortars were also prepared using the NSS aggregate. The first observation is the fact that the ISS aggregate produced higher UCS values than those obtained with the NSS, regardless of the precursor used (50S50F or 100F). These results reinforce the idea that the ISS (as received) can be successfully used as an aggregated, which was previously formulated by other authors [9,10], and could be associated with the development of a good adhesion between the precursor and the ISS particles, as analysed further ahead by BSEM.

Usually, the paste shows higher compressive strength values than its corresponding mortars. However, the 100F(ISS) mortar showed a strength increase, relatively to the 100F paste, of 40%. At the same time, it showed the highest UCS of all the mortars tested, although the most performing paste was the 50S50F (in fact, the 100F paste presented the second lowest UCS of the lot). Such behaviour is most likely related with the fact that the activator / precursor ratio was not optimised for each mixture. For the preparation of the mortars, it was decided to use a unique activator / solid (precursor+aggregate) ratio, of 0.55

(Table 2), to guarantee similar conditions for all the mortars tested. However, this value was established using slump tests [17] on the mortars that showed the highest water adsorption, i.e. 100F(ISS), meaning that while this mortar was prepared with its optimum ratio, the remaining mortars were prepared with a slightly excessive activator content. As a result, 100F(ISS) blends were drier and showed an apparent lower porosity and greater compaction, which probably improved its compressive strength, relatively to the remaining mortars.

3.2. Mineralogical and microstructural characterization

For a thorough microstructural characterisation of the reaction products, paste 50S50F, after 2 and 28 days curing, was selected and analysed using XRD and SEM/EDX. Figure 4 presents the diffractograms of both the paste and the original materials, to allow a direct comparison.

The diffractogram of the ISS-M slag presented several crystalline phases, namely Kirchsteinite, melilite, magnetite and wustite, while the FA-M showed quartz and mullite as its main crystalline phases. All these peaks are still present in the 2 and 28-day diffractograms, indicating that the corresponding phases are practically inert to the alkaline activation process. The fact that their intensity slightly decreased after activation is only a consequence of the material dilution (given the mixture with the activator).

The slag presents a slight halo, between 28 and 38º(2θ), typical of vitreous/amorphous materials, while the fly ash presents a similar halo, although more pronounced, between 20 and 35º(2θ). These halos indicate the existence of a vitreous phase in the precursors,

essential for the development of alkaline activation reactions, due to their reactivity. After activation, and curing for 2 and 28 days, these halos presented significant modifications. They are now not only less intense, but also showing a shift in range, which is now between 20 and 38º(2θ). These changes are a consequence of the formation of essentially amorphous phases in the aluminosilicate gel [18,19], which will partially crystalize, in time (zeolitic precursor). Therefore, and to study the composition of these newly developed material, the pastes were submitted to electron microscopy.

Figure 4: XRD patterns of the milled precursors, FA-M and ISS-M, and the paste 50S50F, after 2 and 28 days curing [ki-kirschsteinite: $CaFe^{2+}(SiO_4)$ PDF 00-034-0098; me-melilite: $Ca_2(Mg_{0.5}Al_{0.5})(Si_{1.5}Al_{0.5}O_7)$ PDF 01-079-2423; mg-magnetite: Fe_3O_4 PDF 00-075-1610; mu-mullite: $Al_6Si_2O_{13}$ PDF 01-079-1453; q-quartz: SiO_2 PDF 01-79-1910; w-wustite: $Fe^{2+}O$ PDF 0-034-0098]

The (50S50F) paste was submitted to SEM observation, after 28 days curing. Figure 5 presents some selected images, which aim to yield information regarding the morphology and overall distribution of the different constituents. Base on all the images presented, it is possible to describe the resulting paste as being compacted, homogenous and with reduced porosity. Several un-reacted particles are partially covered with reaction products (point 1 in Figure 5b and Figure 5c, although some unreacted and 'clean' particles were also found (point 3), implying that the efficiency of the activation promoted during this research work can be further optimised, most likely with a positive impact on mechanical strength.

Figure 5: SEM images of paste 50S50F, cured for 28 days

A quantitative analysis of the pastes developed in the mortars 50S50F(ISS), 50S50F(NSS) and 100F(ISS), after 28 days curing, was performed using BSEM/EDX. These specific mixtures were chosen to allow the comparison between the effects of the two aggregates on the pastes, as well as to analyse the influence of the ISS-M when used in the precursor composition.

The high compaction and reduced porosity of the 50S50F paste, observed when analysing the corresponding SEM images (Figure 5), was transposed to the mortars 50S50F(ISS) (Figure 6) and 50S50F(NSS) (Figure 7). Thus, it is possible to conclude that the addition of the aggregate didn't disturb the general morphology of the original paste. However, the overall aspect of both mortars is significantly different, with the 50S50F(ISS) mortar showing a less defined transition between the aggregate and the surrounding gel, while the 50S50F(NSS) mortar presented a very clear aggregate/gel interface and perfectly intact sand particles, which appear that did not have any type of interaction with the reaction product surrounding them.

The element mapping of the 50S50F(ISS), included in Figure 6, shows the presence, on the bulk gel (areas further away from the gel/particle interfaces) of Al, Fe, Na, Si and Ca, with a prevalence of Na, from the activator, and especially Ca, from the ISS-M. The presence of such elements can be associated with the formation of gel type C-A-S-H or C,N-A-S-H [20–22]. The ISS particles also show strong traces of most of these elements, especially calcium and iron (which is not surprising, given the original composition of the ISS residue), but also silicon, aluminium and sodium, thus indicating a reaction between the particle's surface and the activator. A very different situation, regarding the state of the aggregate particles, was found during the element mapping of the 50S50F(NSS) mortar (included in Figure 7), in the sense that the NSS particles are practically pure silica, showing no signs of participating in the formation of the gel (due to the lack of reaction gel forming on their surface). Furthermore, although a mixture of Na and Ca also dominates the composition of this aluminosilicate gel, it appears that there is a predominant presence of Na (red), relatively to the higher apparent equilibrium between the Na (red) and Ca (yellow) ions in the 50S50F(ISS) bulk gel. This conclusion was numerically confirmed during the analysis of the EDX data regarding the gel composition of each mortar.

Regarding the BSEM images from the mortar 100F(ISS), presented in Figure 8, it is interesting to note that the relation between the aggregate particles and the binding gel is, apparently, more similar to the 50S50F(NSS) mortar than to the 50S50F(ISS) mortar, in the sense that there is a very clear interface between the two areas. Although the interface shows traces of some interconnectivity between the particle's calcium and the sodium and even the silica, from the fly ash-based gel, it is, nevertheless, evident that this gel shows a strong sodium intake, i.e. it is a typical N-A-S-H reaction product [23,24].

Figure 6: BSEM/EDX analysis of the 50S50F(ISS) mortar cured for 28 days

Figure 7: BSEM/EDX analysis of the 50S50F(NSS) mortar cured for 28 days

Figure 8: BSEM/EDX analysis of the 100F(ISS) mortar cured for 28 days

In order to assess the possible influence of the particle/gel interface composition on the mechanical properties of the mortars, the elemental composition of several points located in the interface zone of mortars 50S50F(NSS) (points a1 to a4, Figure 9a) and 100F(ISS) (points b1 to b3, Figure 9b), was quantified and compared with the elemental composition of several points from their respective bulk gel, located on the central areas, away from the aggregate particles (points a5 to a9 and points b4 to b7, respectively). An immediate visual confirmation of the different reactivity levels presented by both aggregates is possible, based on the comparison between the 'clean' surface observed on the NSS particle (Figure 9a) and the high-volume of reaction product covering the ISS particle (Figure 9b). The reactivity of the slag particles is confirmed by the fact that the average calcium content (6.8%) in the interface zone of the 100F(ISS) is 3.4x higher than the average calcium content in the gel (2.0%); while the average calcium content in the interface zone (12.0%) of the mortar 50S50F(NSS) is identical to the average calcium content in the gel (11.9%).

Figure 9: Elemental analysis of the interface zones of the 50S50F(NSS) (a) and 100F(ISS) (b) mortars

To analyse the CaO incorporation in the gel developed in each of the 3 mortars tested, the variation of the CaO/SiO_2 molar ratio with the corresponding Al_2O_3/SiO_2 is presented in Figure 10, and the corresponding averages are shown in Figure 11. Mortar 50S50F(ISS) showed the overall highest CaO content, followed by 50S50F(NSS) and 100FA(ISS), confirming that the slag reacts with the alkaline activator, either as a precursor (finely ground), and as an aggregate.

The reaction of the ISS, in an aggregate role, is clearly observed in mortar 100F(ISS). Based on its Si and Al content, as well as its low Ca content (seen in Figure 8), the binding gel formed in this mortar (resulting exclusively from the alkaline activation of fly ash) is a N-A-S-H gel [18,22]. The presence of higher Ca contents in the gel/particle interface indicates that the slag aggregate provided CaO species, thus creating a transition layer which is almost continuous. On the contrary, the physical separation between the gel and the NSS particles is very clear, even if the gel has a significant supply of Ca (from the ISS-M in the precursor). This difference between the two types of aggregate might have contributed significantly for the overall compressive strength obtained with each one.

Figure 10: Relation between the molar ratios Al_2O_3/SiO_2 and CaO/SiO_2 on the gels developed in mortars 50S50F(ISS), 50S50F(NSS) and 100F(ISS)

Figure 11: Average Al_2O_3/SiO_2, CaO/SiO_2 and Na_2O/Al_2O_3 molar ratios on the gels developed in mortars 50S50F(ISS), 50S50F(NSS) and 100F(ISS)

Regarding the use of ISS-M as a precursor, the results obtained in both pastes and mortars show that this material can be used in the manufacture of alkaline cements, resulting in the development of cementing gels type C-A-S-H or C,N-A-S-H.

4. Conclusions

The present work assessed the suitability of a Portuguese electric arc furnace slag, which has been used as an inert aggregate for the construction of (sub)base layers for road and railway, to be a key constituent in alkali activated cements and mortar composites. It was tested in two distinct roles, namely as a precursor (alone or together with fly ash, after

526 milling) or as an aggregate (used as received). The main conclusions obtained in this paper
527 are:
528
529 • It is possible to use this slag simultaneously as a precursor and as an aggregate. In
530 fact, that duplicity potentiates the mechanical performance of the composite.
531
532 • As a precursor, the finely milled slag reacts with alkaline solutions, allowing the
533 development of a cementitious gel, type C-A-S-H or C,N-A-S-H.
534
535 • Compressive strength data clearly showed that the slag aggregate produced a
536 superior performance, compared with the normalised silica sand, which is a very
537 significant result, in the sense that it opens the possibility of substituting natural
538 aggregates by recycled aggregates, with an actual improvement in terms of
539 technical behaviour.
540
541 • BSEM analysis showed that the more effective performance of the ISS aggregate is
542 due to the absence of a well-defined particle-binder interface and, instead, a well-
543 graduated transition zone was developed, with a very significant calcium content.
544 That Ca was mostly supplied by the aggregate, as showed by the comparison with
545 the BSEM data of the same paste (50S50F) but with silica sand as the aggregate.
546
547 In short, the application of iron and steel slag to alkali activated cement mortars is a viable
548 option, both in terms of sustainability, by avoiding the use of cement and natural
549 aggregates, and by creating an additional destination for this by-product; and in terms of
550 technical efficiency. Furthermore, the possible application solely as an aggregate is also

commendable, not only because the 100FA paste was the most effective binder, but also because it eliminates the need for milling the ISS. The construction industry can and should beneficiate from the introduction of this type of alternative raw materials, not only due to environmental reasons (which constitute, in itself, a powerful motivation), but also because there are potential benefits in terms of technical performance and financial costs. The present study is an example of how the confidence in such materials can be raised, although the moment to move on to the next stage of development is rapidly approaching, especially with the longing urgency to effectively mitigate the landfilling of industrial waste in Europe.

Acknowledgments

The authors would like to acknowledge the contribution of the company DST, SA for a significant logistical support; and the thermoelectric power plant of Pego (Pegop - Energia Eléctrica, Eng. Jorge Henriques), for the supply of the fly ash.

Funding

This work was funded by the R&D Project JUSTREST- Development of Alkali Binders for Geotechnical Applications Made Exclusively from Industrial Waste, with reference PTDC/ECM-GEO/0637/2014, financed by the Foundation for Science and Technology - FCT/MCTES (PIDDAC).

576 **Glossary**

577

AAC	Alkali activated cement
AACO	Alkali activated composite
BF	Blast furnace
BOF	Basic oxygen furnace
BSEM	Back-scattered Electron Microscopy
EAF	Electric arc furnace
FA	Fly ash
FA-M	Milled fly ash
ISS	Iron and steel slag
ISS-M	Milled iron and steel slag
KOH	Potassium hydroxide
LFS	Ladle furnace slag
NaOH	Sodium hydroxide
NSS	Normalised silica sand
Na_2SiO_3	Sodium silicate
PSD	Particle size distribution
SEM	Scanning Electron Microscopy
UCS	Uniaxial compressive strength
XRD	X-ray Diffraction

578

579

580

581 **References**

582

583 [1] Horii K, Kato T, Sugahara K, Tsutsumi N, Kitano Y. Technical Report N109 -
584 Overview of Iron / Steel Slag Application and Development of New Utilization
585 Technologies. 2015.
586 [2] Lee K-J, Yoo S-Y, Koo J-S, Cho B-S, Lee H-H. Experimental Study on the
587 Characteristics of Rapid Chilled Converter Slag by Watering. Int J Concr Struct
588 Mater 2011;5:133–7.
589 [3] World Steel Association. Steel Statistical Yearbook 2016. 2016.
590 [4] World Steel Association. Fact Sheet on Co-Products. WorldsteelOrg 2018:2.
591 [5] Wang WC, Wang HY, Tsai HC. Study on engineering properties of alkali-activated
592 ladle furnace slag geopolymer. Constr Build Mater 2016;123:800–5.
593 [6] Bignozzi MC, Manzi S, Lancellotti I, Kamseu E, Barbieri L, Leonelli C. Mix-design
594 and characterization of alkali activated materials based on metakaolin and ladle slag.
595 Appl Clay Sci 2013;73:78–85.
596 [7] Nguyen H, Carvelli V, Adesanya E, Kinnunen P, Illikainen M. High performance
597 cementitious composite from alkali-activated ladle slag reinforced with
598 polypropylene fibers. Cem Concr Compos 2018;90:150–60.
599 [8] Biskri Y, Achoura D, Chelghoum N, Mouret M. Mechanical and durability
600 characteristics of High Performance Concrete containing steel slag and crystalized
601 slag as aggregates. Constr Build Mater 2017;150:167–78.
602 [9] Coppola L, Buoso A, Coffetti D, Kara P, Lorenzi S. Electric arc furnace granulated
603 slag for sustainable concrete. Constr Build Mater 2016;123:115–9.
604 [10] Khan MSH, Castel A, Akbarnezhad A, Foster SJ, Smith M. Utilisation of steel
605 furnace slag coarse aggregate in a low calcium fly ash geopolymer concrete. Cem

606 Concr Res 2016;89:220–9.

607 [11] Lee JM, Lee YJ, Jung YJ, Park JH, Lee BS, Kim KH. Ductile capacity of reinforced
608 concrete columns with electric arc furnace oxidizing slag aggregate. Constr Build
609 Mater 2018;162:781–93.

610 [12] Ozturk M, Bankir MB, Bolukbasi OS, Sevim UK. Alkali activation of electric arc
611 furnace slag: Mechanical properties and micro analyzes. J Build Eng 2019;21:97–
612 105.

613 [13] Nikolić I, Drinčić A, Djurović D, Karanović L, Radmilović V V., Radmilović VR.
614 Kinetics of electric arc furnace slag leaching in alkaline solutions. Constr Build
615 Mater 2016;108:1–9.

616 [14] ASTM C618. Standard specification for coal fly ash and raw or calcined natural
617 pozzolan for use in concrete. ASTM Int Annu B Stand 2012:1–5.

618 [15] EN 933-1. Tests for geometrical properties of aggregates, Part 1: Determination of
619 particle size distribution - Sieving method. Eur Comm Stand 1997.

620 [16] BSi EN 196-1. Methods of testing cements. Determination of strength. Br Stand
621 Institution, London 2006.

622 [17] ASTM C1437. Standard Test Method for Flow of Hydraulic Cement Mortar. Am
623 Soc Test Mater 2007.

624 [18] Ruiz-Santaquiteria C, Fernández-Jiménez A, Palomo A. Alternative prime materials
625 for developing new cements: Alkaline activation of alkali aluminosilicate glasses.
626 Ceram Int 2016;42:9333–40.

627 [19] Fernández-Jiménez A, Monzó M, Vicent M, Barba A, Palomo A. Alkaline
628 activation of metakaolin–fly ash mixtures: Obtain of Zeoceramics and Zeocements.
629 Microporous Mesoporous Mater 2008;108:41–9.

630 [20] Garcia-Lodeiro I, Fernandez-Jimenez A, Palomo A. Hydration kinetics in hybrid

binders: Early reaction stages. Cem Concr Compos 2013;39:82–92.

[21] García-Lodeiro I, Cherfa N, Zibouche F, Fernández-Jiménez A, Palomo A. The role of aluminium in alkali-activated bentonites. Mater Struct 2015;48:585–97.

[22] Puertas F, Palacios M, Manzano H, Dolado JS, Rico A, Rodríguez J. A model for the C-A-S-H gel formed in alkali-activated slag cements. J Eur Ceram Soc 2011;31:2043–56.

[23] Garcia-Lodeiro I, Fernández-Jimenez A, Pena P, Palomo A. Alkaline activation of synthetic aluminosilicate glass. Ceram Int 2014;40:5547–58.

[24] Torres-Carrasco M, Puertas F. Waste glass in the geopolymer preparation. Mechanical and microstructural characterisation. J Clean Prod 2015;90:397–408.

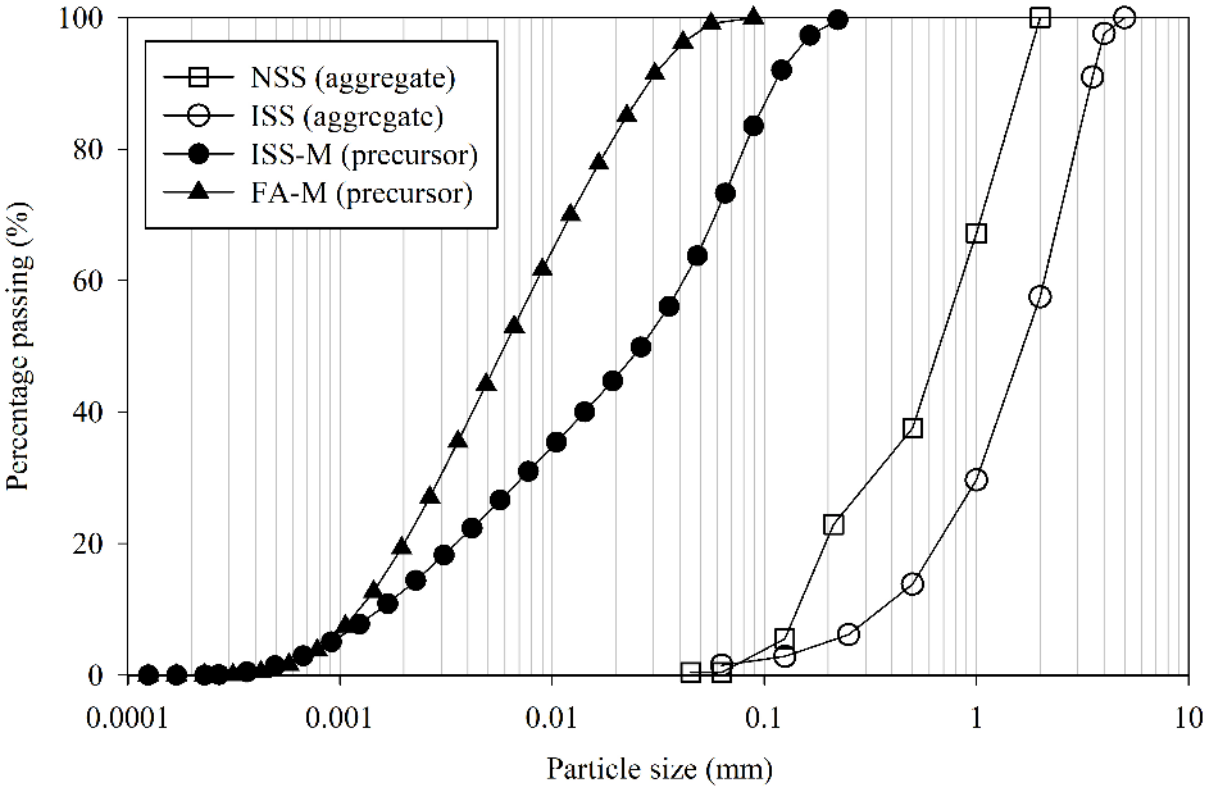

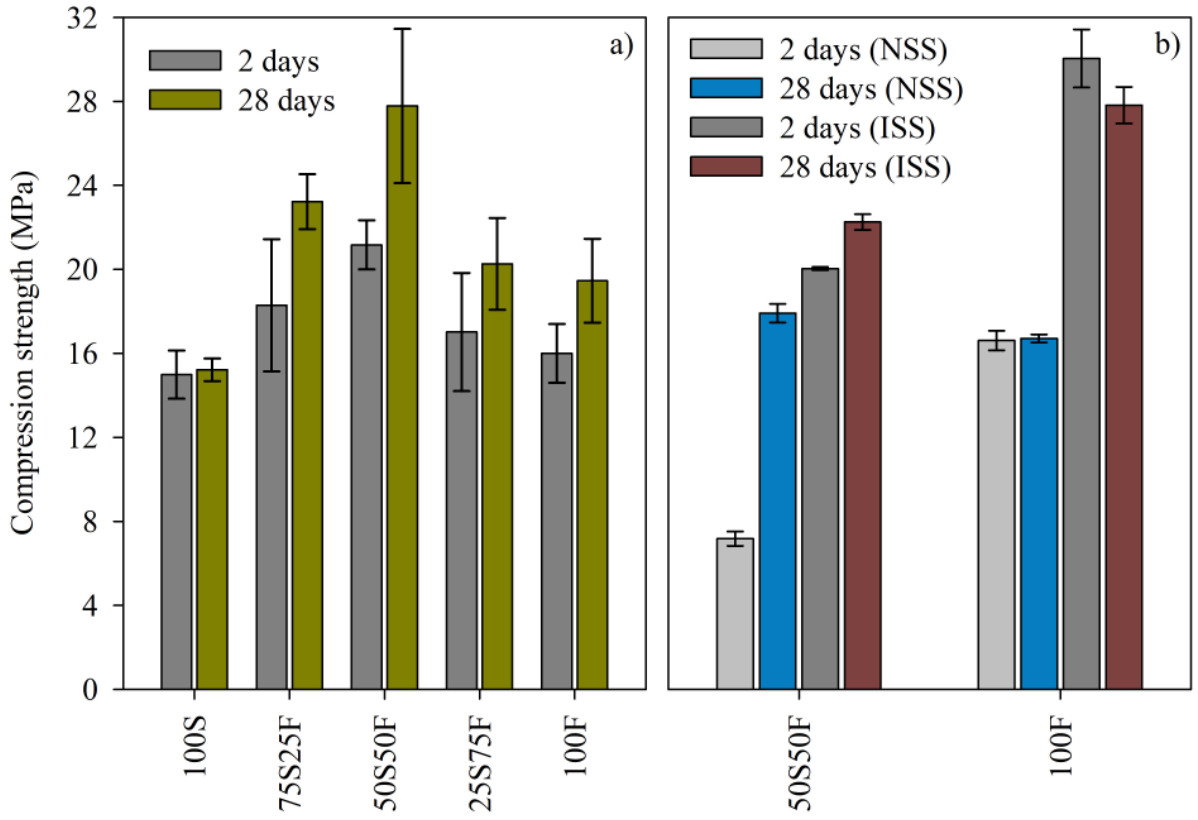
Compression strength (MPa)
0
4
8
12
16
20
24
28
32
a)
2 days
28 days
100S
75S25F
50S50F
25S75F
100F
b)
2 days (NSS)
28 days (NSS)
2 days (ISS)
28 days (ISS)
50S50F
100F

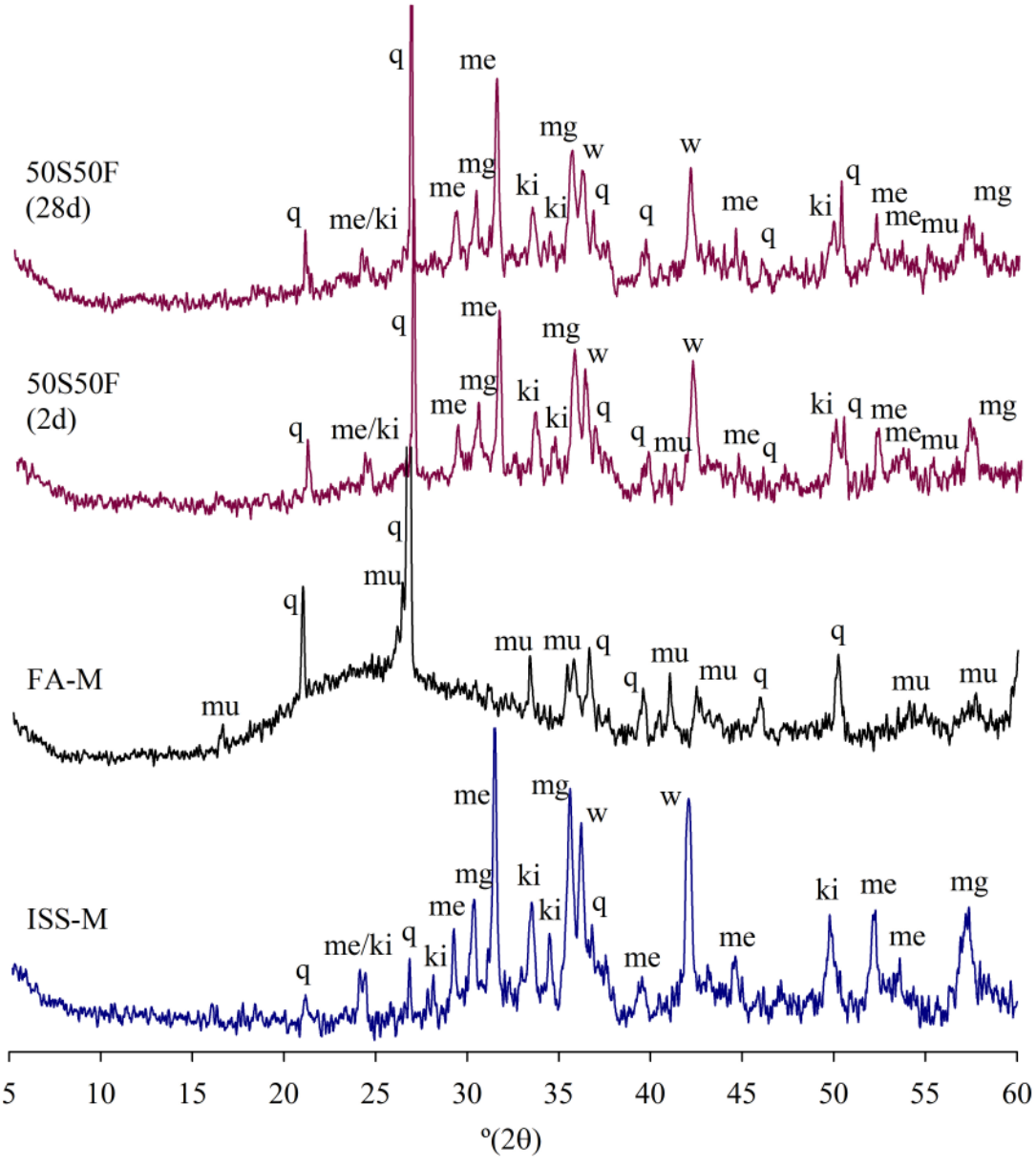
50S50F
(28d)
50S50F
(2d)
FA-M
ISS-M
q
me
mg
w
ki
me/ki
mu
5
10
15
20
25
30
35
40
45
50
55
60
°(2θ)

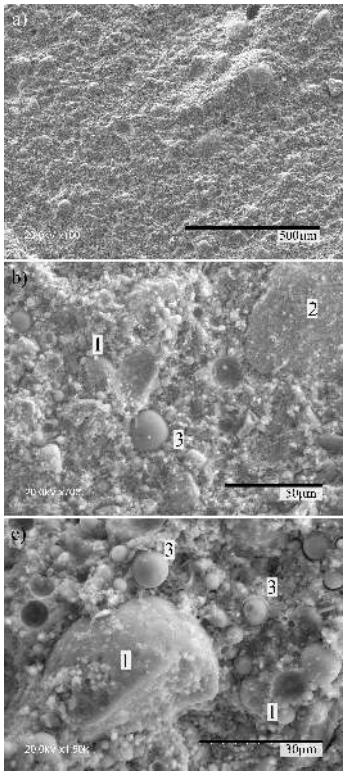

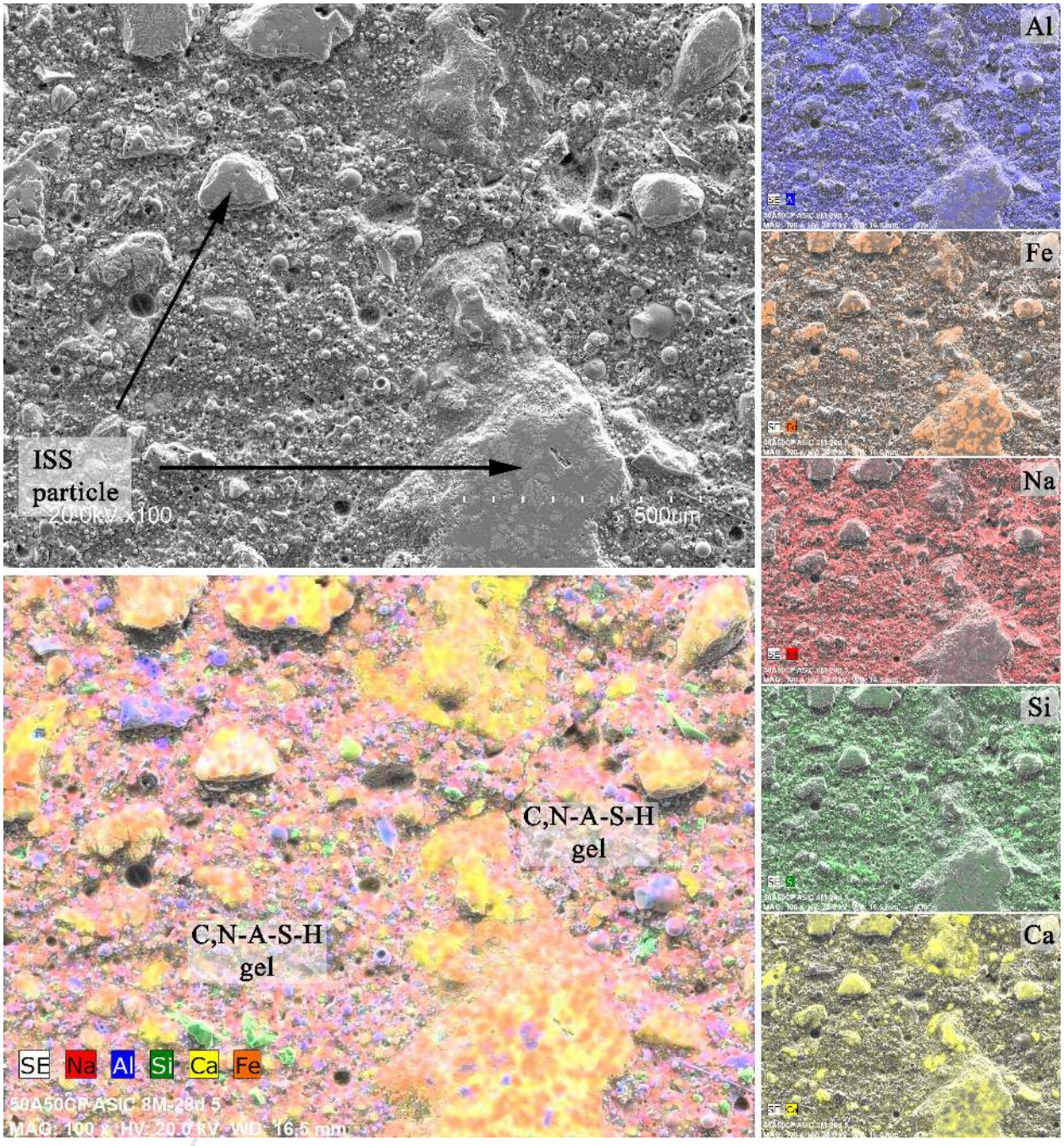
ISS particle
20.0kV x100
500um
Al
Fe
Na
Si
Ca
C,N-A-S-H gel
C,N-A-S-H gel
SE Na Al Si Ca Fe
50A50CP ASIC 8M-28d 5
MAG: 100 x HV: 20.0 kV WD: 16.5 mm

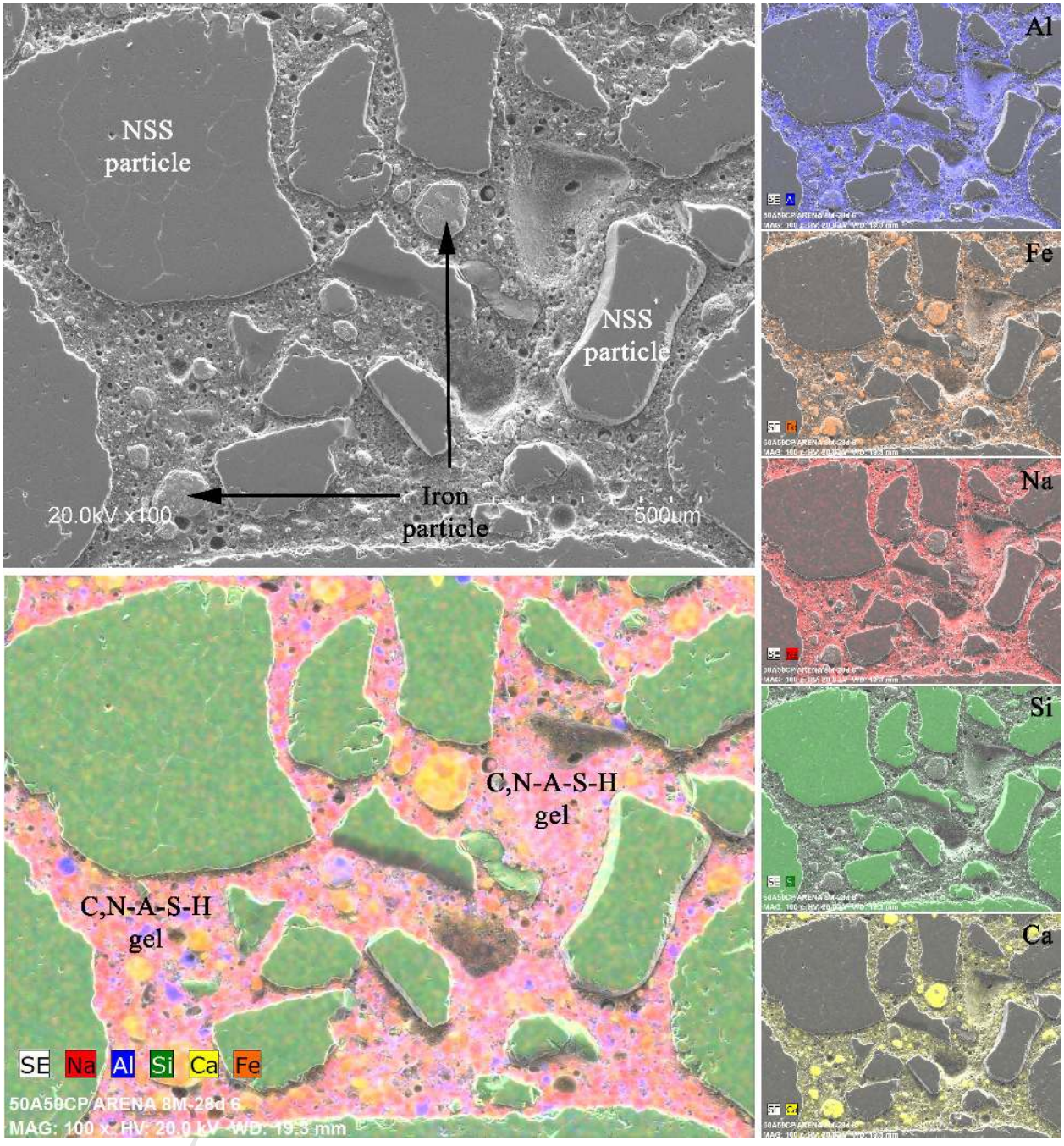
NSS particle
NSS particle
Iron particle
20.0kV x100
500um
C,N-A-S-H gel
C,N-A-S-H gel
SE Na Al Si Ca Fe
Al
Fe
Na
Si
Ca

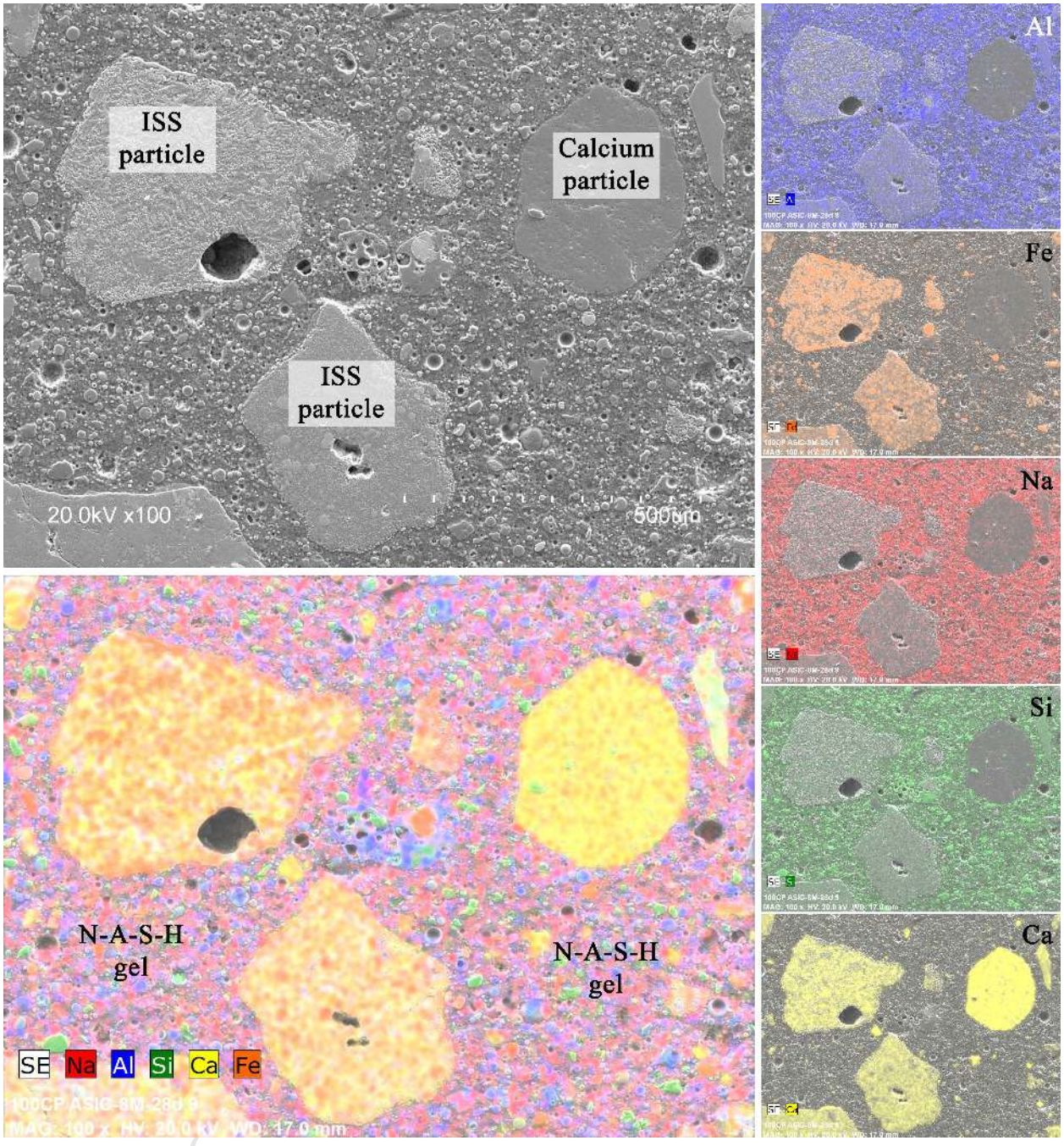
ISS particle
Calcium particle
ISS particle
20.0kV x100
500µm
Al
Fe
Na
Si
Ca
N-A-S-H gel
N-A-S-H gel
SE Na Al Si Ca Fe